UNSTEADY AERODYNAMICS LOADS DURING FLAPPING FLIGHT OF BIRDS; CASE STUDY: STARLING AND SANDPIPER

Ben-Gida[1] H., Stalnov[1] O., Guglielmo[2] C.G., Kopp[3] G.A. and Gurka[4] R.*
*Author for correspondence
[1]Faculty of Aerospace Engineering, Technion - Israel Institute of Technology, Haifa 32000, Israel
[2]Department of Biology, Advanced Facility for Avian Research, Western University, London, Ontario, Canada
[3]Faculty of Engineering, Boundary Layer Wind Tunnel Laboratory, Western University, London, Ontario, Canada
[4]School of Coastal and Marine Systems Science, Coastal Carolina University, Conway, SC 29528, USA
E-mail: rgurka@coastal.edu

ABSTRACT

Flapping wing is one of the most widespread propulsion methods found in nature. However, the current understanding of the bird aerodynamics is incomplete. The role of unsteady motion in the flow and its contribution to the aerodynamics is still an open question. The current study deals with the estimation of unsteady aerodynamic forces on freely flying birds through analysis of wingbeat kinematics and near wake flow measurements using long duration time-resolved particle image velocimetry. Two bird species have been investigated, the starling and sandpiper. Using long-time sampling data, several wingbeat cycles have been analyzed in order to cover both the downstroke and upstroke phases of flight. Lift and drag were obtained using the momentum equation for viscous flows and were found to share a highly unsteady behavior. The two birds show similar behavior during the downstroke phase of flight, whereas the sandpiper was shown to have a district signature during its upstroke phase. The contribution of the circulatory lift component is shown to be significant when estimating lift (or power) of birds in flapping flight. Moreover, the unsteady drag term was found to have a crucial role in the balance of drag (or thrust), particularly during transition phases. These findings may shed light on the flight efficiency of birds by providing a partial answer to how they minimize drag and maximize lift during flapping flight.

INTRODUCTION

Flapping flight is one of the most complex yet widespread propulsion methods found in nature. Although aeronautical technology has advanced remarkably over the past century, flying animals still demonstrate higher efficiency [1–3]. One of the key open questions is the role of unsteady fluid motion in the wake of flying animals and its contribution to the forces acting during the downstroke and upstroke phases of flight [4]. The unsteady flow over small–scale wings has gained significant attention recently both in the study of bird and insect flight as well as for development advanced aerodynamic models for high-performance micro-aerial vehicles [2].

As living organisms, birds are subject to selective pressures; as such, one may assume they flap their wings in a highly efficient manner. This notion is supported by the tendency of birds, as well as many other animals, to operate in a limited Strouhal number range between 0.2 and 0.4 [5, 6]. To model the time dependent aerodynamic lift force acting on a section of a wing L' it is natural to start with a quasi–steady approach. Most studies on the aerodynamics of natural flyers [7–10] have utilized this approach and estimate the lift force from PIV (Particle Image Velocime-

NOMENCLATURE

A	[m]	Vertical displacement of a wing section
AR	[-]	Aspect ratio ($= b^2/S_{ref}$)
b	[m]	Wing span (tip to tip)
c	[m]	Root wing chord length
D'	[N/m]	Drag force per unit length acting on a wing section
D'_0	[N/m]	Steady drag component
D'_1	[N/m]	Unsteady drag component
f	[Hz]	Flapping frequency
L'	[N/m]	Lift force per unit length acting on a wing section
L_0	[N/m]	Quasi-steady lift component
L_1	[N/m]	Added mass lift component
L_2	[N/m]	Wake-induced lift component
L_C	[N/m]	Circulatory lift component; $= L_0 + L_2$
p	[Pa]	Pressure
p_∞	[Pa]	Freestream pressure
Re	[-]	Reynolds number ($= \rho U_\infty c/\mu$)
S	[m^2]	Surface area of a control volume V
S_{ref}	[m^2]	Wings area
St	[-]	Strouhal number ($= A_0 f/U_\infty$)
t	[sec]	Time variable
U_∞	[m/sec]	Freestream velocity
$\vec{u}$	[m/sec]	Velocity vector
u	[m/sec]	Streamwise velocity component
V	[m^3]	Control volume for the momentum equation
v	[m/sec]	Vertical velocity component
w	[m/sec]	Spanwise velocity component
x	[m]	Cartesian streamwise axis direction
y	[m]	Cartesian vertical axis direction
z	[m]	Cartesian spanwise axis direction

Special characters

α	[degrees]	Freestream angle of attack
Γ	[m^2/sec]	Bound circulation
γ	[m/sec]	Vorticity distribution about a lifting surface
γ_w	[m/sec]	Vorticity distribution in the wake
ρ	[kg/m^3]	Freestream air density
μ	[Pa·sec]	Freestream dynamic viscosity
ω_z	[1/sec]	Spanwise vorticity

try), in the Trefftz or streamwise-normal planes, behind flying birds through applying the classical Kutta–Joukowski theorem, $L' = \rho U_\infty \Gamma$; here, ρ is the fluid density, U_∞ is the freestream velocity, and Γ is the bound circulation, which can be calculated from the vorticity field. For estimating the quasi–steady lift, it is sufficient to capture a portion of, or an entire, wingbeat cycle, where the circulation is computed from a single instantaneous vector map [11] or from synchronized velocity maps triggered to match various phases within the wingbeat cycle [12]. Moreover, using several consecutive velocity maps of which a full wingbeat cycle has been reconstructed, one can estimate the lift from a series of velocity fields capturing the far wake behind a freely flying bird [8,10]. Yet, analysis incorporating the unsteady effects in estimation of lift is lacking. One of the challenges in estimating the evolution of lift over time is the need to measure the wake using a technique that introduces high spatial and temporal resolution over a relatively long period of time.

Recently, Ben–Gida *et al.* [13] studied the near wake of freely flying European starling using long duration time–resolved Particle Image Velocimetry (hereafter PIV) [14]. Wakes of four complete wingbeat cycles were reconstructed from the PIV images in the near wake, enabling comparison of steady and unsteady drag components deduced from the velocity profiles in the wakes. It was demonstrated that the negative contribution of the unsteady drag component at the transition stages (downstroke to upstroke and vice verse) of the wingbeat phase reduces the total drag during the flapping motion of the starling. Stalnov *et al.* [15] extended the study by Ben–Gida *et al.* [13] and estimated the time dependent lift from the wake flow field measurements of the starling. Two methods were applied to estimate the lift; the first is the unsteady thin airfoil theory [16,17] and the second method is based on the derivation of the aerodynamic forces directly from the momentum equations [18]. Both methods demonstrated that the time dependent lift components cannot be assumed negligible and should be considered when estimating lift (or power) of birds during flapping flight.

Many of the aerodynamic models for birds are based on fixed wings in steady flow [19]. The current study addresses the near wake variations behind freely flying birds in time and space with a particular focus on the unsteady aerodynamics that results from the flapping motion. The goal of the present work is to evaluate and compare the unsteady aerodynamics in the wake of a freely flying European starling (*Sturnus vulgaris*) and a western sandpiper (*Calidris mauri*) from long-duration time-resolved PIV measurements. This comparison can shed light on the significant role of unsteady aerodynamics during birds locomotion.

MATHEMATICAL MODELING

Drag Force

Consider a two–dimensional wing section of a bird surrounded by a control volume V and enclosed by the surface area S, with its width in the spanwise y direction being unity. Inside the control volume, the streamwise x–component of the momentum equation can be re–written to express the drag force per unit span:

$$D' = -\rho \frac{\partial}{\partial t} \iiint_V u dV - \rho \oiint_S (\vec{u} \cdot dS) u - \iint_S (p \cdot dS)_x \quad (1)$$

where $\vec{u} = (u, v, w)$ is the velocity vector in Cartesian coordinate system and p is the pressure. Note that the viscous terms have been neglected as they scale with Re^{-1}. Defining S to be sufficiently far from the wing, where the pressure is assumed equal to p_∞, and after substituting the continuity equation into Eq. 1, the drag force per unit span can be written as follows [13]:

$$D' = \underbrace{\rho \int_0^h u(U_\infty - u) \mathrm{d}y}_{D'_0 \text{ - Steady term}} - \underbrace{\rho \frac{\partial}{\partial t} \int_0^h \int_0^l u \mathrm{d}x \mathrm{d}y}_{D'_1 \text{ - Unsteady term}} \quad (2)$$

The steady drag component D'_0, as it appears in Eq. 2, is referred to the velocity deficit drag in classical aerodynamics, whereas the unsteady drag component D'_1 is added due to the flapping motion. While the steady drag term can be easily obtained from near wake velocity field, the unsteady drag term requires information regarding the entire control surface surrounding the wing section. In the current study, we assume most of the unsteady disturbances generated by the flapping motion can be obtained from the velocity field in the near wake. Thus, we approximate the full surface integral of the unsteady term to include only the velocity field obtained from the PIV experiments in the near wake of the freely flying birds. Here, h and l are the vertical and horizontal extent of the computed velocity field in the wake, respectively.

Lift Force

Any unsteady motion of a lifting surface is accompanied with shedding of vortices into the wake. Assuming potential flow, one can utilize the unsteady thin airfoil theory [16,17], which assumes a planar wake evolution, to compute the time-dependent lift of a two-dimensional lifting surface with acceptable precision. Accordingly, an expression for the time dependent lift force (per unit span) of a two-dimensional lifting surface can be written as the sum of three terms:

$$\begin{aligned} L' = & \underbrace{\rho U_\infty \Gamma}_{L_0 \text{ - Quasi-steady term}} - \underbrace{\rho \frac{\partial}{\partial t} \int_{-1}^{1} x\gamma(x,t)\, \mathrm{d}x}_{L_1 \text{ - Added mass term}} \\ & \underbrace{+ \rho U_\infty \int_1^\infty \frac{\gamma_w(x,t)}{\sqrt{x^2-1}} \mathrm{d}x}_{L_2 \text{ - Wake-induced lift term}} \end{aligned} \quad (3)$$

where $x = -1$ and $x = 1$ are the leading– and trailing–edge locations, respectively. The first term in Eq. 3 represents the quasi–steady lift L_0 produced by the instantaneous bound circulation Γ.

The second term L_1 represents the added mass contribution and it results from the inertia of the fluid moving with the lifting surface. Finally, the third term is the induced lift component L_2 that produced by the wake vorticity. In the near wake of flapping birds the flow structures can be simplified, thus allowing the use of the planar wake assumption and consequently the unsteady thin airfoil theory. Although general trends may be well described with the use of such theory, it is the small scales in the wake that actually of interest. When analyzing these vortical structures in the near wake of flying birds, one can deduced that a more precise viscous–based method is required for the lift estimation.

Therefore, the time-dependent lift generated during the flapping motion of the freely flying birds has been evaluated from the near wake velocity fields by utilizing Wu's viscous flow approach [18], which is based on the Navier–Stokes equations [21, 22]. Neglecting the added mass term, the time–dependent lift force according to Wu's approach can be expressed as:

$$L'(t) = -\rho \frac{d}{dt} \iint x\omega_z(t)\, \mathrm{d}x\mathrm{d}y \tag{4}$$

where the term $\iint x\omega_z(t)\, \mathrm{d}x\mathrm{d}y$ is the first x-moment of the vorticity. The spanwise vorticity $\omega_z(t)$ at the wake is defined as:

$$\omega_z(t) = \frac{\partial v}{\partial x} - \frac{\partial u}{\partial y} \tag{5}$$

and is evaluated directly from the PIV data using a least squares differentiation scheme [26]. Here u and v are streamwise and transverse velocity components, respectively.

Following Theodorsen [16] we can identify the expression in Eq. 4 as the circulatory lift component L_C, which is the sum of the quasi–steady and wake–induced lift components ($L_C = L_0 + L_2$). Applying Taylor's hypothesis, $\mathrm{d}x = U_\infty \mathrm{d}t$, one can transform the spatial derivative in Eq. 4 into a temporal one. Moreover, since at the beginning of the flapping cycle the lift is unknown we shall refer to the estimated lift component as an increment in the circulatory lift that is generated from the beginning of the cycle, thus equal to $\Delta L_c(t)$ that can be expressed as:

$$\Delta L_c(t) = \rho U_\infty \int \zeta(t)\, \mathrm{d}t. \tag{6}$$

In order to estimate the circulatory lift $\Delta L_c(t)$ from Eq. 6 one needs to acquire information regarding the vorticity flux $\zeta(t)$ in the near wake:

$$\zeta(t) = \int U_c \omega_z(t)\, \mathrm{d}y. \tag{7}$$

The vorticity flux, defined by Eq. 7 is estimated for each individual velocity map obtained in the near wake of the freely flying birds as function of time. The calculated vorticity flux corresponds to the spanwise vorticity component and is integrated over a selected region in each velocity map.

EXPERIMENTAL SETUP

Wind Tunnel

Experiments were conducted in a hypobaric climatic wind tunnel at the Advanced Facility for Avian Research (AFAR) at Western University. The wind tunnel is closed-loop type with an octagonal test section, characterized with a cross-sectional area of 1.2m^2 and width, height and length of 1.5m, 1m, and 2m, respectively. The control of speed, pressure, temperature, and humidity in the wind tunnel enables simulation of flight conditions at high altitudes as experienced by birds during long distance migratory travel. The flight conditions reported in this work correspond to atmospheric static pressure, a temperature of 15°C, and relative humidity of 80%. A more detailed description of the wind tunnel, the experimental technique can be found in Ben-Gida *et al.* [13] and Kirchhefer *et al.* [14].

The Birds

Following the studies by Ben-Gida *et al.* [13] and Kirchhefer *et al.* [14], new measurements were sampled in the wake of a freely flying European starling (*Sturnus vulgaris*) and a western sandpiper (*Calidris mauri*). The birds flight characteristics are given in Table 1. A collection of optoisolators operated by six infrared transceivers were integrated into the PIV system, in order to prevent direct contact between the birds and the laser sheet (while they were flying in the wind tunnel). The optoisolators triggered the laser only when the birds were flying upstream the PIV field of view. All animal care and procedures were approved by the University of Western Ontario Animal Use Sub-Committee (protocols 2006-011, 2010-216).

Bird	U_∞ [m/sec]	m [g]	b [m]	c [cm]	AR	St	$Re \times 10^4$
European starling	13.5	76	38	6	6.4	0.3	5.4
western sandpiper	10	30	26	4.5	7.5	0.13	3.1

Table 1: Flight characteristics of the birds in the wind tunnel

Long duration time resolved PIV

Flow measurements were taken using a long-duration time-resolved PIV system developed by Taylor *et al.* [23]. The PIV system consists of a 80W double-head diode-pumped Q-switched Nd:YLF laser at a wavelength of 527nm and two CMOS cameras (Photron FASTCAM-1024PCI) with spatial resolution of 1024×1024pixel^2 at a sampling rate of 1000Hz. The PIV system is capable of acquiring image pairs at 500Hz using two cameras for a continuous period of 20 minutes. Olive oil aerosol particles, 1μm in size on average [24], were introduced into the wind tunnel

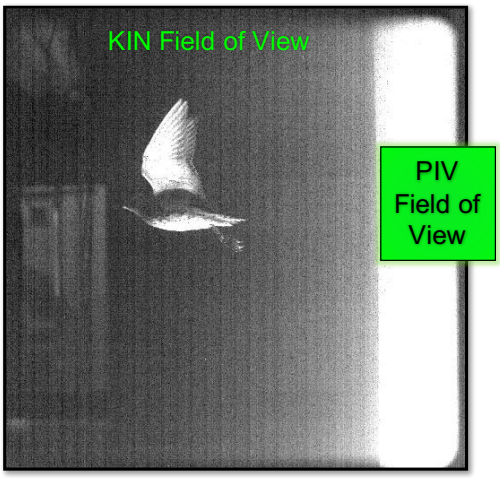

Figure 1: **Field of view setup of both the PIV and KIN cameras.**

using a Laskin nozzle from the downstream end of the test section so that it did not cause a disturbance to the flow in the test section or to the birds. The system is designed to work either in a two-dimensional or Stereo mode. Herein, we used one camera for the PIV whilst a second one for measuring the wingbeat kinematics simultaneously with the PIV. The PIV camera's field of view was $12\times12\text{cm}^2$ (corresponding to $2c\times2c$ and $2.5c\times2.5c$ for the starling and sandpiper, respectively). The velocity fields were computed using OpenPIV [23] using $32\times32\text{pixel}^2$ interrogation windows with 50% overlap, yielding a spatial resolution of 32 vectors per average chord, equal to 1.8 vectors per millimeter. In the current experiments, measurements were taken 2 chord lengths and 3 chord lengths behind the starling and sandpiper, respectively. The wakes were sampled in the streamwise-normal plane at 2ms intervals (500Hz), therefore, both the downstroke and the upstroke phases of the two birds were temporally resolved.

Kinematic measurements

To relate the wake measurements to the kinematic motion of the bird's wings, an analysis of the kinematic motion has been undertaken. The field of view by the kinematic CMOS camera (henceforth referred to as 'KIN') was $9c\times9c$ in the experiments with the starling (corresponding to 50×50 cm^2) and $11c\times11c$ in the experiments with the sandpiper (corresponding to 50×50 cm^2).

RESULTS AND DISCUSSION

The data discussed herein was selected from a broad acquisition batch where the birds were flying continuously for a few seconds. The selection criterion was based on the flight mode chosen: a steady flapping mode with no net acceleration of the birds over a wingbeat cycle. In the current study, we present and characterize two wakes, one for each bird investigated. Each wake corresponds to one wingbeat cycle, which includes a downstroke and an upstroke phase.

Wakes Characteristics

The wakes of both the starling and the sandpiper are characterized in terms of aerodynamic forces and vorticity content. To determine if the vorticity, as measured in the near wake, is sufficient for the force estimations, the peak vorticity in the current data behind the birds are compared with that from previous works [4,8,10,11]. Peak normalized vorticity $\omega_z c/U_\infty$ of 3.4 and 1.1 were found for the starling and sandpiper, respectively. These values are comparable with the peak vorticity values found from birds and bats flying at various speeds (see [13] for more information).

Wake Reconstruction In the current study, the near wake flow fields were captured simultaneously with the bird's kinematic motion, allowing one to relate the wake structures to the kinematics of the birds. A visualization of each wingbeat cycle is performed by generating a wake composite image from multiple PIV realizations, which will shed light on the wake structures that manifest the aerodynamic forces. The procedure was performed using PIV data collected at a sampling rate of 500Hz - significantly higher than the wingbeat frequencies of the bird (see Table 1). As a result, a vorticity pattern appearing in one frame would also appears in the consecutive frame, but phase–shifted. The wake composite is formed by plotting sequential instantaneous vorticity fields computed from PIV data and by matching shifted patterns in the vorticity fields. The offset of the n^{th} successive PIV images is calculated as $U_c\cdot\Delta t\cdot n$. The convection velocity U_c is the velocity at which the characteristics of the wake collectively travel downstream. Here, wake composites have been generated using the free-stream velocity U_∞ as a convection velocity.

The generation of a wake composite provides a useful tool for observing the time–series of measurements representing the wake of a wingbeat cycle. The wake structures that appear 'downstream' in the wake composite image happen earlier in time, while the structures that appear 'upstream' in the composite happen later in time. The generation of the wake composite image invokes similar argument to Taylor hypothesis [27] in which the characteristics of the flow are advected through the field of view, where the offset of one image to the next is based on the free stream speed. It is noteworthy that the typical offset $U_c\cdot\Delta t\cdot n$ between consecutive images is $0.4c$ (starling) or $0.5c$ (sandpiper) and an instantaneous PIV measurement has a spatial dimension of $2c$ (starling) or $2.5c$ (sandpiper). Hence, at any location in the wake composite image, there are several overlapping images that can be used to ascertain the instantaneous wake characteristics over the streamwise distance of the PIV window to compare with the wake composite at the same location.

Wake Evolution The wakes features are presented through fluctuating normalized spanwise vorticity fields as depicted in Figures 2 and 3, for both the starling and the sandpiper. The wakes are presented as if the birds were flying from the right side to left side of the image. The measurement plane in the current study is significantly closer to the birds in the streamwise direction, thus allowing one to have a better view of the vortical struc-

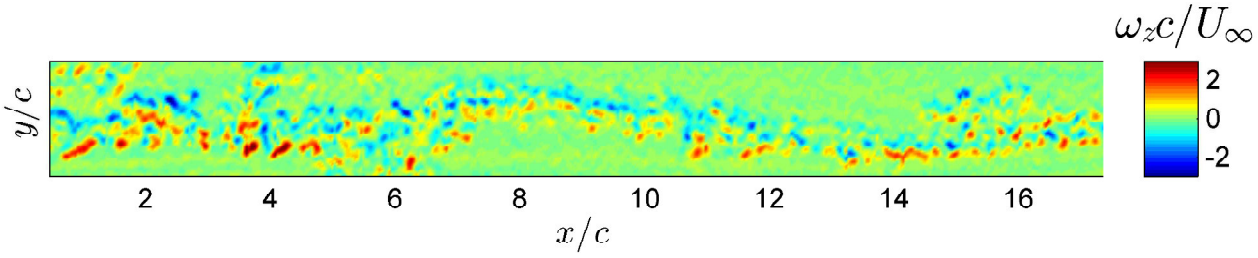

Figure 2: **Reconstruction of the starling's wake vorticity as thought the bird flies from right to left.**

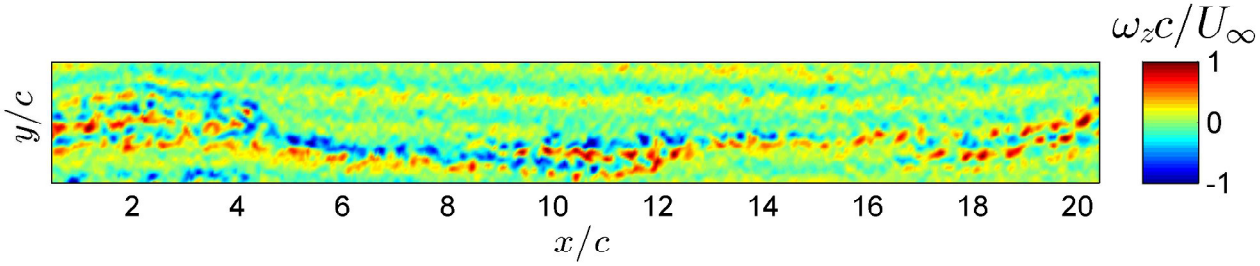

Figure 3: **Reconstruction of the sandpiper's wake vorticity as thought the bird flies from right to left.**

tures generated by the birds.

One may note the periodicity of the wakes over the shedding cycle, where, as would be expected, the top half of each wake is composed primarily of negative spanwise vorticity and the bottom half by positive spanwise vorticity. Comparing the wakes of the two birds we can note that the starling generates higher vorticity values compare to the sandpiper (nearly three times higher). This may be related to the lower size and mass of the sandpiper, which needs to generate less lift (and therefore also less vorticity) than the starling. In addition, during the upstroke phase (roughly the left half of each wake) it appears the starling generates large structures of vorticity that are accompanied with high strength, whereas the sandpiper produces smaller vortices with lower strength. Such difference in the wake signature can be attributed to the different flying kinematics of the two birds during their upstroke phase. Figures 4-5 depicts the starling and the sandpiper, as they were flying inside the wind tunnel, at the end of their upstroke phase. One can observe the sandpiper was fully retracting its wings upwards, whereas the starling was not. This can explain the larger more stronger structures of vorticity observed in the starling's wake. In the next section, the wake data are used to quantitatively examine the sectional drag force as derived from Eq. 2.

Drag Estimates

The variation of the drag force was estimated from the wake data of both birds, according to Eq. 2. In the current study, each drag component (steady and unsteady) was normalized by the dynamic pressure times the wing root chord ($0.5\rho U_\infty^2 c$) of each bird to obtain the sectional drag coefficient C_d instead of the drag force per unit span D'. Thus, the drag generated by the birds is comparable. Figures 6 and 7 describe the time variation of the steady (C_{d_0}), unsteady (C_{d_1}), and total sectional drag coefficient (C_d) for the wingbeat cycles depicted in Figures 2 and 3. The downstroke phase is denoted with a a white background, whereas the upstroke phase with a gray background.

The drag integrals were performed for each instantaneous velocity field characterizing the wake of the birds. For C_{d_0}, different streamwise velocity profiles were sampled at different x-positions for each velocity field map. Subsequently, these profiles within one PIV vector map were spatially averaged into one profile describing the velocity deficit, similar to the procedure described in Ben–Gida *et al.* [13]. The process performs a somewhat spatial window averaging that smooth out some of the variations within each vector map. Each point in Figures 6 and 7 represents the integral value depicted from each velocity field yielding a time evolution of the sectional drag coefficient in the near wake.

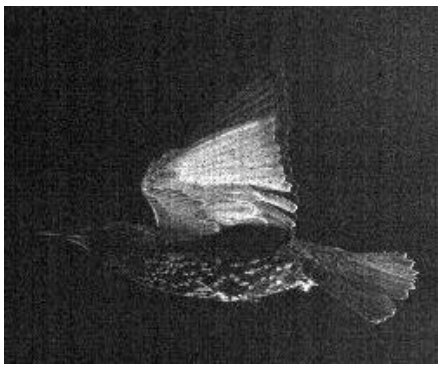

Figure 4: **Starling, as it was captured in the wind tunnel, at the end of its upstroke phase.**

As a validation stage for the data obtained in these experiments, the steady and unsteady drag components were calculated for the startling (see Figure 6) and compared to the results reported by Ben–Gida *et al.* [13]. Good agreement was found,

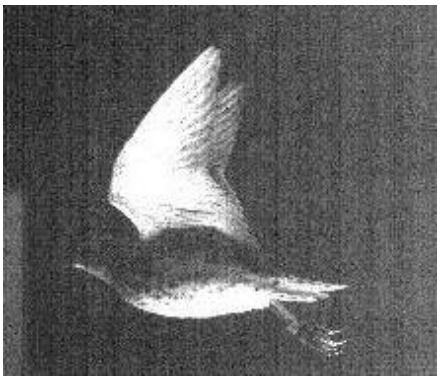

Figure 5: **Sandpiper, as it was captured in the wind tunnel, at the end of its upstroke phase.**

which supports the new data obtained. By examining Figures 6-7, one can notice the drag coefficient varies in a non-periodic manner. This is mainly due to the kinematics of the wings, which undergoes a unique unsteady motion involving both translation and rotation. In addition, distinct similarities and differences of the steady and unsteady components of the two birds can be depicted. In agreement with the results reported by Ben–Gida *et al.* [13], the steady drag of both birds is shown to be positive throughout most of the wingbeat cycle except for the transition from downstroke to upstroke. It is noteworthy that a wider range of negative steady drag values were depicted for the sandpiper transition phase (see Figure 7). In addition, while the variation of the steady drag component during the downstroke phase is roughly similar between the two birds, during the upstroke phase the steady drag component of the starling shows much higher values. Different trend in the upstroke phase between the two birds was also found in the unsteady contribution to the drag, as depicted in Figures 6-7. Therefore, higher sectional drag coefficients are depicted for the starling (~ 0.4), as compared to the sandpiper (~ 0.2).

The low drag generated by the sandpiper during its upstroke phase can be related to its kinematic motion, as discussed aforesaid (see Figure 4). In contrast to the starling, the sandpiper is known for its unique ability as a long distance migrating bird [28]. The sandpiper presumably adapted for migration flights by reducing the drag penalty during its flapping flight; thereby, minimizing the energy cost required for the long distances it needs to cover. In the next section, the lift force is computed from the wake data obtained in the current experiments.

Lift Estimates

During the steady phase of flight the bird's weight must be balanced by an equal amount of lift [29], generated during a wingbeat cycle. Figures 8 and 9 show the circulatory lift produced by the starling and sandpiper, respectively. One can observe that the the minimum lift values are produced during the transition from upstroke to downstroke phase. The physical argument to this observation is that during the upstroke to downstroke transition the bird folds its wings, causing them to stop acting as lifting surfaces, and thus generates almost no lift and drag (see Figures 6 and 7). The aforesaid results imply that the usage of quasi–steady

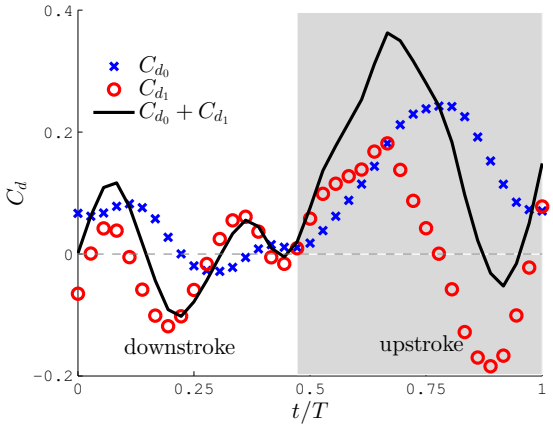

Figure 6: **Estimation of the starling's drag.**

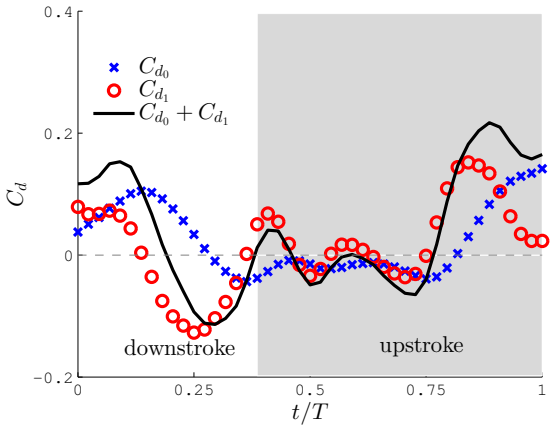

Figure 7: **Estimation of the sandpiper's drag.**

lift theory might result in underestimating the lift that a bird is actually generates during flapping flight.

Moreover, one may observe the circulatory lift generated during the downstroke phase by both birds is roughly similar in value. However, during the upstroke phase, large variation in the circulatory lift is observed for the starling. This observation further supports the results obtained in the former section.

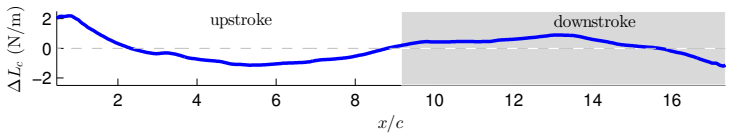

Figure 8: **Estimation of the starling's circulatory lift component.**

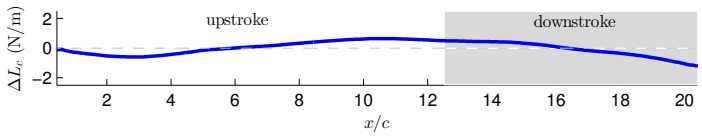

Figure 9: **Estimation of the sandpiper's circulatory lift component.**

CONCLUSIONS

In this study, a long-duration time-resolved PIV system was used to obtain time-resolved measurements of the velocity field in the wake of a freely flying bird in flapping mode at the AFAR hypobaric wind tunnel. Two birds were studied herein, a European starling (*Sturnus vulgaris*) and a western sandpiper (*Calidris mauri*). The wake topologies of the birds were reconstructed based on patterns from the instantaneous vorticity fields where the measurement plane of the velocity was close to the wing root of the birds. Both drag and lift forces were obtained using the momentum equation for viscous flows.

Results show both similarities and differences in the flow signature for each bird, which is highly dependent on their flapping motion. The sandpiper resulted a lower drag force during its upstroke phase than the starling due to its unique ability as a long distance migrating bird. The circulatory lift results support this conclusion as depicted from Figures 8 and 9. It is deduced that the unsteady portion of the flow, as shown in this study, have an important role on the bird's flight efficiency.

REFERENCES

[1] Zheng L., Hedrick T. and Mittal R., A comparative study of the hovering efficiency of flapping and revolving wings, Bioinspir Biomim 8: 036001, 2013

[2] Shyy W., Lian Y., Tang J., Viieru D. and Liu H., Aerodynamics of low Reynolds number flyers. Cambridge University Press, 2008

[3] Floreano D., Zuffere J.C., Srinivasan M.V. and Ellington C., Flying Insects and Robots. Springer, 2009

[4] Hedenström A. and Spedding G.R., Beyond robins: aerodynamic analyses of animal flight. J R Soc Interface, Vol. 5, 2008, pp. 595-601

[5] Anderson J.M., Streitlien K., Barrett D.S. and Triantafyllou M.S. Oscillating foils of high propulsive efficiency. Journal of Fluid Mechanics, Vol. 360, 1998, pp. 41-72

[6] Taylor G.K., Nudds R.L. and Thomas A.L.R., Flying and swimming animals cruise at a Strouhal number tuned for high power efficiency. Nature, Vol. 425(6959), 2003, pp. 707-711

[7] Henningsson P., Muijres F.T. and Hedenström A., Time-resolved vortex wake of a common swift flying over a range of flight speeds. J R Soc Interface, Vol. 8, 2010, pp. 807-816

[8] Spedding G.R., Rosén M. and Hedenström A., A family of vortex wakes generated by a thrush nightingale in free flight in a wind tunnel over its entire natural range of flight speeds. Journal of Experimental Biology, Vol. 206, 2003, pp. 2313-2344

[9] Henningsson P., Hedenström A. and Bomphrey R.J., Efficiency of lift production in flapping and gliding flight of swifts, PLOS ONE, Vol. 9, 2014, e90170

[10] Hedenström A., Rosén M., Spedding G.R., Vortex wakes generated by robins Erithacus rubecula during free flight in a wind tunnel. Journal of the Royal Society Interface, Vol. 3, 2006, pp. 263-276

[11] Henningsson P., Spedding G.R. and Hedenström A., Vortex wake and flight kinematics of a swift in cruising flight in a wind tunnel. Journal of Experimental Biology, Vol. 211, 2008, pp. 717-730

[12] Muijres F.T., Johansson L.C., Winter Y. and Hedenström A., Leading edge vortices in lesser long-nosed bats occurring at slow but not fast flight speeds. Bioinspiration and Biomimetics, Vol. 9, 2014, 025006

[13] Ben-Gida H., Kirchhefer A.J., Taylor Z.J., Bezner-Kerr W., Guglielmo C.G., Kopp G.A. and Gurka R., Estimation of Unsteady Aerodynamics in the Wake of a Freely Flying European Starling (Sturnus vulgaris). PLOS ONE, Vol. 8(11), 2013, e80086

[14] Kirchhefer A.J., Kopp G.A. and Gurka R. The near wake of a freely flying European starling. Physics of Fluids, Vol. 25(5), 2013, 051902

[15] Stalnov O., Ben-Gida H., Kirchhefer A.J., Guglielmo C.G., Kopp G.A., Liberzon A. and Gurka R., On the Estimation of Time Dependent Lift of a European Starling (Sturnus vulgaris) during Flapping Flight. PLOS ONE, Vol. 10(9), 2015, e0134582

[16] Theodorsen T., General theory of aerodynamic instability and the mechanism of flutter, NACA TR-496, 1935, pp. 291-311

[17] von Kármán T. and Sears W.R., Airfoil theory for non-uniform motion. Journal of the Aeronautical Sciences, Vol. 5(10), 1938, 379-390

[18] Wu J.C., Theory for aerodynamic force and moment in viscous flows. AIAA, Vol. 19(4), 1981, pp. 432âĂŞ441

[19] Hubel T.Y. and Tropea C., The importance of leading edge vortices under simplified flapping flight conditions at the size scale of birds. J Exp Biol, Vol. 213, 2010, pp. 1930-1939

[20] Leishman J.G., Principles of helicopter aerodynamics. Cambridge University Press, 2006

[21] Batchelor G., An Introduction to Fluid Dynamics. Cambridge University Press, 1967

[22] Lamb H., Hydrodynamics. Dover, New York, 1945

[23] Taylor Z.J., Gurka R., Kopp G.A. and Liberzon A. Long-duration time-resolved PIV to study unsteady aerodynamics. IEEE Transactions on Instrumentation and Measurement, Vol. 59(12), 2010, pp. 3262-3269

[24] Echols W.H., Young J.A., Studies of portable air-operated aerosol generators. US Naval Research Laboratory Washington, DC, 1963

[25] Liberzon A., Gurka R. and Hetsroni G., Vorticity characterization in a turbulent boundary layer using PIV and POD analysis. In: Proceeding of 4th International Symposium on PIV, GÃűttingen, Germany, 2001

[26] Raffel M., Willert C., Wereley S.T. and Kompenhans J., Particle Image Velocimetry: a practical guide. Springer, 2007

[27] Taylor G.I., The spectrum of turbulence. Proceedings of the Royal Society of London. 164, 476-490, 1938

[28] Iverson G.C., Warnock S.E., Butler R.W, Bishop M.A. and Warnock N, Spring migration of Western sandpipers along the pacific coast of north America: A telemetry study. The Condor 98, 10-21, 1996

[29] Pennycuick, C. J., The mechanics of bird migration. Ibis 111(4), 525-556, 1996